CHINESE OPTICS LETTERS

Vol. 22, No. 3 | March 2024

Broadband second-harmonic generation in thin-film lithium niobate microdisk via cyclic quasi-phase matching

Jiefu Zhu (朱杰夫)[1], Tingting Ding (丁婷婷)[2], Xuerui Sun (孙雪芮)[1], Fengchao Ni (倪枫超)[1], Hao Li (黎 浩)[1], Shijie Liu (刘时杰)[1], Yuanlin Zheng (郑远林)[1,3*], and Xianfeng Chen (陈险峰)[1,3,4**]

[1] State Key Laboratory of Advanced Optical Communication Systems and Networks, School of Physics and Astronomy, Shanghai Jiao Tong University, Shanghai 200240, China

[2] School of Electronic and Electrical Engineering, Shanghai University of Engineering Science, Shanghai 201620, China

[3] Shanghai Research Center for Quantum Sciences, Shanghai 201315, China

[4] Collaborative Innovation Center of Light Manipulations and Applications, Shandong Normal University, Jinan 250358, China

*Corresponding author: ylzheng@sjtu.edu.cn

**Corresponding author: xfchen@sjtu.edu.cn

Received October 8, 2023 | Accepted November 16, 2023 | Posted Online March 22, 2024

Whispering-gallery-mode (WGM) microresonators can greatly enhance light–matter interaction, making them indispensable units for frequency conversion in nonlinear optics. Efficient nonlinear wave mixing in microresonators requires stringent simultaneous optical resonance and phase-matching conditions. Thus, it is challenging to achieve efficient frequency conversion over a broad bandwidth. Here, we demonstrate broadband second-harmonic generation (SHG) in the *x*-cut thin-film lithium niobate (TFLN) microdisk with a quality factor above 10^7 by applying the cyclic quasi-phase-matching (CQPM) mechanism, which is intrinsically applicable for broadband operation. Broadband SHG of continuous-wave laser with a maximum normalized conversion efficiency of ∼15%/mW is achieved with a bandwidth spanning over 100 nm in the telecommunication band. Furthermore, broadband SHG of femtosecond lasers, supercontinuum lasers, and amplified spontaneous emission in the telecommunication band is also experimentally observed. The work is beneficial for integrated nonlinear photonics devices like frequency converters and optical frequency comb generator based on second-order nonlinearity on the TFLN platform.

Keywords: lithium niobate; whispering-gallery mode; broadband second-harmonic generation; cyclic quasi-phase matching.

DOI: 10.3788/COL202422.031903

1. Introduction

Optical parametric processes based on the second-order nonlinearity ($\chi^{(2)}$) are common ways to achieve frequency conversion both in classical and quantum regimes. As a multifunctional ferroelectric crystal, lithium niobate ($LiNbO_3$ or LN) not only has a broad transparent window, stable physical and chemical properties, but also large second-order nonlinearity and electro-optic effect, which has been the backbone of such applications for over seven decades. Recently, the emerge of the thin-film lithium niobate (TFLN) platform has propelled the development of integrated nonlinear photonics as well as LN-based devices to a new height[1–6]. Various high-performance nonlinear devices on the novel platform have been demonstrated using different geometries[7–13]. Among these, whispering-gallery-mode (WGM) microresonators are indispensable units for frequency conversion, as they can confine light in a small volume for a long time and greatly enhance light–matter interaction.

Efficient nonlinear wave mixing requires phase matching, i.e., energy and momentum conservation. Typically, the condition can only be met in a narrow wavelength range due to dispersion and becomes even more stringent in WGM microresonators as double (triple, or even multiple) resonance and phase matching should be satisfied simultaneously. Frequency conversion in nonlinear microresonators can reach an extremely high efficiency if the condition is perfectly fulfilled, especially in high quality (Q) microring cavities[12,13]. Along with microrings, microdisks are often used to achieve efficient wavelength conversion in a wide range due to its high mode density and easier implementation for phase matching. With the advance of micro-/nanofabrication techniques, the Q factor of TFLN

microdisks has reached the order of 10^8[14], close to the theory limit. Strong nonlinear optical processes have been realized in TFLN microdisks, such as second-harmonic generation (SHG)[15,16], sum-frequency generation (SFG)[17–19], cascaded harmonic generation[20,21], cascaded four-wave mixing[22], and spontaneous parametric downconversion[23].

In particular, TFLN is also an ideal platform for optical frequency comb (OFC) generation and is promising for direct self-referencing. Generally, there are two different methods for on-chip frequency comb generation. The most common method is based on Kerr nonlinearity ($\chi^{(3)}$) for spectral broadening. One important development for TFLN-based Kerr combs is to obtain an octaves-spanning comb that allows for $f-2f$ self-referencing, which could be simplified by the intracavity SHG process[24,25]. The other method is quadratic frequency comb generation, which arises from a back-to-back OPO cascaded with SHG or SFG. The process may also proceed in the reverse case (SHG or SFG followed by OPO)[26–28]. Broadband SHG for quadratic frequency combs has always been difficult, since efficient wavelength conversion is required across a wide wavelength range with strong dispersion.

In this work, we achieve broadband SHG in the x-cut TFLN microdisk with a high Q factor of 3.32×10^7 by utilizing the scheme of cyclic quasi-phase matching (CQPM). The broadband SHG is observed using different sources including a continuous-wave (cw) laser, femtosecond (fs) laser, supercontinuum (SC) laser, and amplified spontaneous emission (ASE) in the telecommunication band. A high normalized conversion efficiency of 15.2%/mW is achieved using a cw pump, and the efficient conversion spans a wide range of over 100 nm. These results show the strong capability of TFLN microdisks for integrated nonlinear frequency converter application in a universal way. Our work also suggests great potential for realizing quadratic OFC generation.

2. Experimental Results and Discussion

In the x-cut LN microdisk, the efficient broadband SHG is realized when the pump and its second-harmonic (SH) waves are both TE (transverse-electric) modes and the phase-matching configuration is ee–e type to access the largest element d_{33} of the second-order nonlinear susceptibility of LN. This can be achieved in experiment by controlling the polarization of the input to excite the specific WGM mode. The effective nonlinear coefficient can be expressed as $d_{\text{eff}}=-d_{22}\cos^3\theta+3d_{31}\cos^2\theta\cdot\sin\theta+d_{33}\sin^3\theta$, where d_{22}, d_{31}, and d_{33} are the corresponding tensor elements of the second-order susceptibility, respectively. θ is the azimuthal angle and is also the wave vector k orientation with respect to the optical axis (z axis). Due to the birefringence of LN, the TE-polarized (extraordinary) wave experiences a θ-dependent refractive index and effective nonlinear coefficient, as shown in Fig. 1(a). This mechanism mimics the quasi-phase-matching (QPM) scheme and is called cyclic quasi-phase matching (CQPM). The advantage of the scheme is that the phase matching can be naturally satisfied in a broad bandwidth[15].

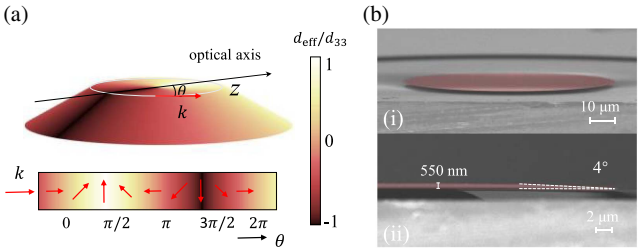

Fig. 1. (a) Effective nonlinear coefficient d_{33} varies with the azimuthal angle θ in an x-cut TFLN microdisk; (b) false-colored SEM images of the TFLN microdisk viewed at different angles.

The microdisk used in our experiment is fabricated using an ion-sliced x-cut TFLN wafer (NANOLN). A top layer of x-cut single crystalline TFLN with a thickness of 600 nm is bonded to a silica buffer layer of 2 μm thickness, and the hold is a 0.5-mm-thick LN substrate. The TFLN microdisk is fabricated utilizing ultraviolet lithography and chemo-mechanical polishing (CMP) with an extremely smooth sidewall and a small wedge angle of approximately 4°. The sample fabrication is conducted at the Center for Advanced Electronic Materials and Devices, SJTU. The scanning electron microscopy (SEM) topography of the microdisk sample is shown in Fig. 1(b). The thickness of the LN film is reduced to 550 nm after a second CMP procedure. The freestanding LN microdisk on a silica pedestal is formed after erosion by a buffered oxide etch (BOE) solution. The fabrication process is similar to that in CMP lithography reported by others, but our mask patterning method is different. Details about the CMP lithography can be found in Refs. [19,29,30]. The diameter of our x-cut LN microdisk is approximately 100 μm and that of the silica pedestal is about 50 μm. Large microdisks have high mode density, as they are supportive for higher-order WGM modes, which can facilitate simultaneous resonance for different waves during nonlinear mixing.

The experimental setup for the nonlinear optical experiments is schematically illustrated in Fig. 2(a). The pump is, respectively, launched from a cw, fs, SC laser, and ASE in the communication band. A variable optical attenuator (VOA) is used to tune the output power. An inline polarization controller (PC) is used to control the light polarization. The pump power is divided into two channels by a single-mode fiber coupler (Coupler1). One arm is launched into a tapered fiber, which is placed in contact with the microdisk to evanescently couple light into the TFLN microdisk, through which the SHG signal (as well as the residual pump) is coupled out of the microdisk. The TFLN microdisk is placed on a three-dimensional nanostage to finely control its coupling with the tapered fiber. Meanwhile, the other arm of the input pump is monitored by a power meter. The tapered fiber is made by heating and pulling a single-mode fiber to a waist diameter of ~1 μm. A 780/1550-nm wavelength-division multiplexer (WDM) is used at the end of the tapered fiber to separate the pump and its SHG signal. The output 1550 nm pump light is monitored using an InGaAs photodetector (PD) and an oscilloscope. The 780 nm pump

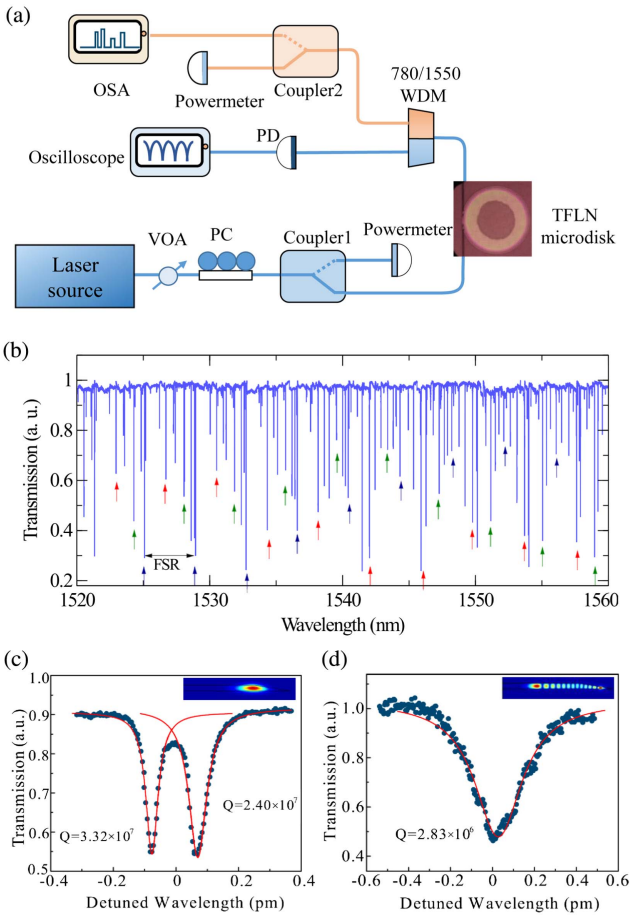

Fig. 2. (a) Schematic of the experimental setup; (b) transmission spectrum of the TFLN microdisk. (c), (d) Lorentzian fitting of the resonances at 1563.3 and 781.7 nm, revealing a loaded Q factor of 3.32×10^7 and 2.83×10^6, respectively.

signal is sent to another fiber coupler (Coupler2), one arm of which is monitored by an optical spectrum analyzer (OSA); the other is sent to a power meter to simultaneously record the signal power. An optical microscope (not shown in the figure) is adopted during the whole experiment for coupling optimization and observing the scattered SHG emission. The transmission spectrum and the measurement of the Q factor of the microdisk are obtained by scanning the cw laser wavelength without thermal broadening at low input power of 0.5 μW, as shown in Fig. 2(b). The same family of different order TE modes is marked with the same color arrows. The measured free spectral range (FSR) is 3.8 nm, consistent with the theoretical prediction of 3.7 nm. The loaded Q factor of our TFLN microdisk is determined to be 3.32×10^7 by Lorentz fittings of the resonance at the wavelength of 1563.3 nm near critical coupling condition, as shown in Fig. 2(c). The mode splitting is attributed to backscattering, which is also an indicator of the high Q of the cavity[31,32]. The Q factor at the SH wavelength of 781.7 nm is measured to be 2.83×10^6, as shown in Fig. 2(d). The coupling efficiency is much lower than that at the FW wavelength due to unoptimized coupling condition.

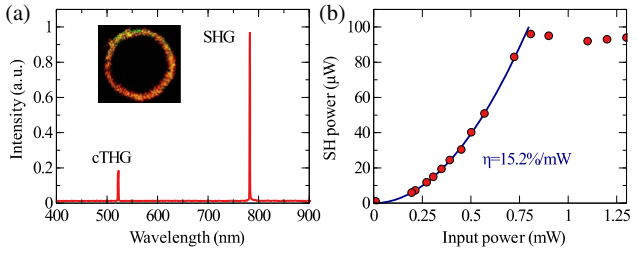

Fig. 3. Experimental results of SHG in the TFLN microdisk. (a) Spectrum of the SHG and cTHG; (b) SH power as a function of the cw pump.

In our experiment, strong visible emission scattered from the TFLN microdisk could be observed when the cw pump wavelength is tuned to each cavity resonance. Figure 3(a) shows the observed spectrum of the SHG signal at the wavelength of 782.2 nm (the pump wavelength is 1564.3 nm). Cascaded third-harmonic generation (cTHG), i.e., simultaneous SHG and SFG of FW and the generated SH, is also observed in the experiment. The relation of the SHG signal power, P_{SH}, and the pump power, P_{pump}, is shown in Fig. 3(b). The measured SHG power grows quadratically with the increasing pump power until P_{SH} reaches saturation. The saturation is mainly due to thermal shift of the resonance under increased power in the cavity. P_{SH} is the power of the SH signal outcoupled from the microdisk (loss of Coupler2, WDM, and tapered fiber is considered) and P_{pump} is the input pump power measured at the Coupler1 output port. By quadratic fitting of data points below 0.8 mW, the normalized SHG conversion efficiency of our microdisk is calculated to be 15.2%/mW. The actual SHG conversion efficiency in the cavity is much higher than this value. The obtained efficiency can be further increased if the SH out-coupling efficiency is improved.

The SHG process in the TFLN microdisk is observed to be phase-matched in a broad bandwidth, which is a direct result of the CQPM scheme. Figure 4(a) shows the recorded SHG spectra as the wavelength of the cw pump is scanned from 1510 to 1630 nm (the whole tunable range of the laser), with an interval of ~1 nm. Figure 4(b) shows the SHG spectra as the pump wavelength is finely tuned, with an interval of ~0.1 nm from 1550 to 1552 nm. It should be noted that the SHG spectrum for each pump wavelength is recorded at optimized coupling

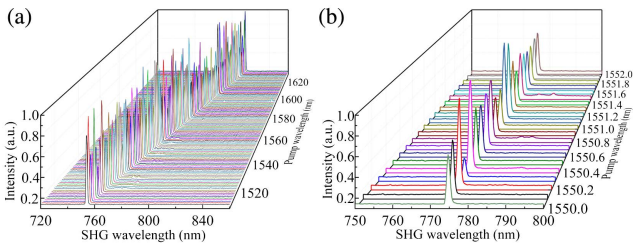

Fig. 4. Experimental results of broadband SHG in the TFLN microdisk using tunable cw pump. (a), (b) Spectra of broadband SHG with a wavelength interval of 1 and 0.1 nm, respectively.

condition at the cavity's resonance, which may not be strictly equidistantly-spaced due to dispersion. According to the results, our high-Q TFLN microdisk shows strong ability for efficient nonlinear conversion, which provides significant promise for direct SHG of broadband light.

Then, we investigate the performance of our TFLN microdisk using broadband light sources. Coupling of wideband light into high-Q microresonators can be highly inefficient, as only a small fraction of frequency components can be coupled into and resonant in the cavity. Remarkably, broadband SHG could still be observed using fs, SC laser, and ASE in our experiment. The spectra of the fs laser before (blue line) and after (red line) coupling with the microdisk are shown in Fig. 5(a). The fs laser is a mode-locked pulsed fiber centered at 1556 nm, with a pulse duration of 500 fs and a repetition rate of 60 MHz. Figure 5(b) shows the spectrum of the broadband SHG generated by the fs pump with a bandwidth of ~10 nm. The comb lines of the spectrum are unresolvable using the spectrometer, whose resolution is only 0.3 nm. The SHG as a function of the input fs power is shown in Fig. 5(c), which shows a quadratic relation with a normalized conversion efficiency of 3.5×10^{-5} mW^{-1}. Saturation is not observed because the coupling efficiency is much lower than that of the cw pump, and the conversion efficiency is therefore reduced.

The situation is similar when the pump is an SC laser. The seed laser is a picosecond mode-locked fiber laser at 1064 nm with a pulse duration of 6 ps and a repetition rate of 80 MHz. Its spectrum is then broadened via the SC generation process to an ultrabroad range of 410–2400 nm. The SC source is filtered by a long-pass filter (1300 nm) before entering the microdisk. Figure 5(d) shows the spectra of the SC laser pump (1300–1675 nm) before (blue line) and after (red line) coupling with the microdisk. The spectrum at the long wavelength is truncated at the detected limit of the OSA. The spectrum of broadband SHG is shown in Fig. 5(e), indicating a bandwidth of ~150 nm. As shown in Fig. 5(f), the observed SHG signal generated by the SC laser is quadratically dependent on the incident SC pump power, and the normalized SHG conversion efficiency pumped by the SC laser is calculated to be about 3.0×10^{-5} mW^{-1}. The comb-shaped spectra of the coupled and generated light cannot be resolved by the spectrometer. The low conversion efficiencies are attributed to the inefficiency light coupling of the wide bandwidth sources. However, it can be envisioned that the current scheme holds significant promise for frequency-doubling of OFC if it is realized in the TFLN microdisk. And if OFC is directly generated in the microdisk, the conversion efficiency can be much higher.

More remarkably, broadband SHG can also be observed using an ASE pump. The spectra of the ASE pump before (blue line) and after (red line) coupling with the microdisk are shown in Fig. 5(g). Figure 5(h) shows the spectra of broadband SHG generated by the ASE pump with a bandwidth of ~7 nm. The SHG as a function of the input ASE power is shown in Fig. 5(i), which shows a normalized SHG conversion efficiency of about 8.0×10^{-8} mW^{-1}. The efficiency for ASE, i.e., partially coherent light, is much lower than that of lasers.

There are several reasons leading to the fact that not all the spectral components of the wideband light are frequency-doubled during the experiment. First, the coupling condition is not always optimized over a wide range. Second, the comb line spacing (or repetition rate) is not fully compatible with the resonances of the microdisk in a wide range. Third, the polarization state is not fully controlled for the wideband lasers, and for the ASE source, the polarization of the light is randomized. Nevertheless, the results surely show that the x-cut TFLN microdisk based on CQPM is highly valuable for efficient broadband frequency conversion.

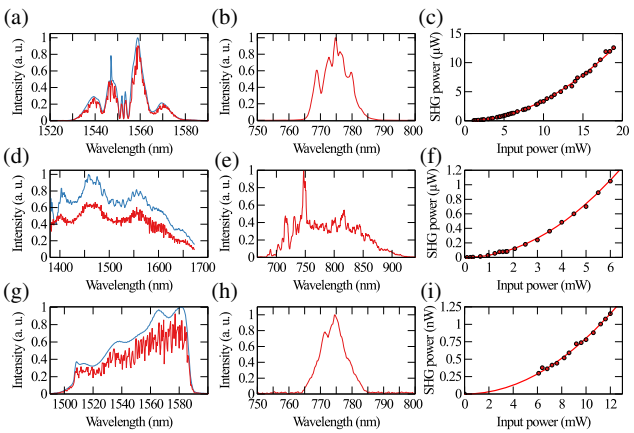

Fig. 5. Experimental results of the broadband SHG pumped by fs, SC laser, and ASE in the TFLN microdisk. (a) Spectra of the fs laser before and after coupling into the microdisk; (b) broadband SHG of fs laser; (c) SH power varies with respect to the incident fs pump. (d) Spectra of the SC laser before and after coupling into the microdisk; (e) broadband SHG of the SC laser; (f) SH power varies with respect to the incident SC pump. (g) Spectra of the ASE before and after coupling into the microdisk; (h) broadband SHG of ASE; (i) SH power varies with respect to the incident ASE pump.

3. Conclusion

In conclusion, we have demonstrated broadband CQPM SHG in the x-cut high-Q TFLN microdisk. The broadband SHG is observed using a cw, fs, SC laser, and ASE with efficient conversion. The result would be beneficial for integrated nonlinear photonics devices like frequency converters on the TFLN platform.

Acknowledgements

This work was supported by the National Natural Science Foundation of China (Nos. 12074252, 12192252, and 62022058), the National Key Research and Development Program of China (No. 2022YFA1205101), the Shanghai Municipal Science and Technology Major Project (No. 2019SHZDZX01-ZX06), and the Yangyang Development Fund.

References

1. A. Boes, L. Chang, C. Langrock, *et al.*, "Lithium niobate photonics: unlocking the electromagnetic spectrum," Science **379**, eabj4396 (2023).
2. A. Honardoost, K. Abdelsalam, and S. Fathpour, "Rejuvenating a versatile photonic material: thin-film lithium niobate," Laser Photonics Rev. **14**, 2000088 (2020).
3. Y. Li, Z. Huang, W. Qiu, *et al.*, "Recent progress of second harmonic generation based on thin film lithium niobate [Invited]," Chin. Opt. Lett. **19**, 060012 (2021).
4. Y. Zheng and X. Chen, "Nonlinear wave mixing in lithium niobate thin film," Adv. Phys. X **6**, 1889402 (2021).
5. R.-R. Xie, G.-Q. Li, F. Chen, *et al.*, "Microresonators in lithium niobate thin films," Adv. Opt. Mater. **9**, 2100539 (2021).
6. J. Lin, F. Bo, Y. Cheng, *et al.*, "Advances in on-chip photonic devices based on lithium niobate on insulator," Photonics Res. **8**, 1910 (2020).
7. X. Sun, Y. Wu, C. Lu, *et al.*, "Experimental investigation on the unbalanced Mach–Zehnder interferometer on lithium niobate thin film," Chin. Opt. Lett. **20**, 101301 (2022).
8. L. Wang, X. Zhang, and F. Chen, "Efficient second harmonic generation in a reverse-polarization dual-layer crystalline thin film nanophotonic waveguide," Laser Photonics Rev. **15**, 2100409 (2021).
9. Q. Guo, R. Sekine, L. Ledezma, *et al.*, "Femtojoule femtosecond all-optical switching in lithium niobate nanophotonics," Nat. Photonics **16**, 625 (2022).
10. M. Li, H. Liang, R. Luo, *et al.*, "High-*Q* 2D lithium niobate photonic crystal slab nanoresonators," Laser Photonics Rev. **13**, 1800228 (2019).
11. J. Ma, F. Xie, W. Chen, *et al.*, "Nonlinear lithium niobate metasurfaces for second harmonic generation," Laser Photonics Rev. **15**, 2000521 (2021).
12. J.-Y. Chen, Z.-H. Ma, Y. M. Sua, *et al.*, "Ultra-efficient frequency conversion in quasi-phase-matched lithium niobate microrings," Optica **6**, 1244 (2019).
13. J. Lu, M. Li, C.-L. Zou, *et al.*, "Toward 1% single-photon anharmonicity with periodically poled lithium niobate microring resonators," Optica **7**, 1654 (2020).
14. R. Gao, H. Zhang, F. Bo, *et al.*, "Broadband highly efficient nonlinear optical processes in on-chip integrated lithium niobate microdisk resonators of q-factor above 10^8," New J. Phys. **23**, 123027 (2021).
15. J. Lin, N. Yao, Z. Hao, *et al.*, "Broadband quasi-phase-matched harmonic generation in an on-chip monocrystalline lithium niobate microdisk resonator," Phys. Rev. Lett. **122**, 173903 (2019).
16. Z. Hao, L. Zhang, W. Mao, *et al.*, "Second-harmonic generation using d_{33} in periodically poled lithium niobate microdisk resonators," Photonics Res. **8**, 311 (2020).
17. Z. Hao, J. Wang, S. Ma, *et al.*, "Sum-frequency generation in on-chip lithium niobate microdisk resonators," Photonics Res. **5**, 623 (2017).
18. X. Ye, S. Liu, Y. Chen, *et al.*, "Sum-frequency generation in lithium-niobate-on-insulator microdisk via modal phase matching," Opt. Lett. **45**, 523 (2020).
19. J. Zhu, X. Sun, T. Ding, *et al.*, "Sum-frequency generation in a high-quality thin film lithium niobate microdisk via cyclic quasi-phase matching," J. Opt. Soc. Am. B **40**, D44 (2023).
20. S. Liu, Y. Zheng, and X. Chen, "Cascading second-order nonlinear processes in a lithium niobate-on-insulator microdisk," Opt. Lett. **42**, 3626 (2017).
21. L. Zhang, Z. Hao, Q. Luo, *et al.*, "Dual-periodically poled lithium niobate microcavities supporting multiple coupled parametric processes," Opt. Lett. **45**, 3353 (2020).
22. S. Liu, Y. Zheng, Z. Fang, *et al.*, "Effective four-wave mixing in the lithium niobate on insulator microdisk by cascading quadratic processes," Opt. Lett. **44**, 1456 (2019).
23. B.-Y. Xu, L.-K. Chen, J.-T. Lin, *et al.*, "Spectrally multiplexed and bright entangled photon pairs in a lithium niobate microresonator," Sci. China Phys. Mech. Astron. **65**, 294262 (2022).
24. Y. Okawachi, M. Yu, B. Desiatov, *et al.*, "Chip-based self-referencing using integrated lithium niobate waveguides," Optica **7**, 702 (2020).
25. L. Chang, S. Liu, and J. E. Bowers, "Integrated optical frequency comb technologies," Nat. Photonics **16**, 95 (2022).
26. J. Szabados, D. N. Puzyrev, Y. Minet, *et al.*, "Frequency comb generation via cascaded second-order nonlinearities in microresonators," Phys. Rev. Lett. **124**, 203902 (2020).
27. X. Wang, K. Jia, M. Chen, *et al.*, "2-μm optical frequency comb generation via optical parametric oscillation from a lithium niobate optical superlattice box resonator," Photonics Res. **10**, 509 (2022).
28. I. Ricciardi, S. Mosca, M. Parisi, *et al.*, "Optical frequency combs in quadratically nonlinear resonators," Micromachines **11**, 230 (2020).
29. R. Wu, J. Zhang, N. Yao, *et al.*, "Lithium niobate micro-disk resonators of quality factors above 10^7," Opt. Lett. **43**, 4116 (2018).
30. M. Wang, R. Wu, J. Lin, *et al.*, "Chemo-mechanical polish lithography: a pathway to low loss large-scale photonic integration on lithium niobate on insulator," Quantum Eng. **1**, e9 (2019).
31. D. S. Weiss, V. Sandoghdar, J. Hare, *et al.*, "Splitting of high-*Q* Mie modes induced by light backscattering in silica microspheres," Opt. Lett. **20**, 1835 (1995).
32. J. Zhu, S. K. Ozdemir, Y.-F. Xiao, *et al.*, "On-chip single nanoparticle detection and sizing by mode splitting in an ultrahigh-*Q* microresonator," Nat. Photonics **4**, 46 (2010).